

The drag on a vertically moving grid of bars in a linearly stratified fluid

R.C. Higginson, S.B. Dalziel, P.F. Linden

678

Abstract We present the results of an investigation of the drag force on a horizontal grid of bars moving vertically through a stratified fluid. A novel approach was used to calculate the drag, based on measurements of the terminal velocity of a freely rising grid. In the homogeneous case the drag coefficient of the grid is found to be approximately constant for a range of grid-based Reynolds numbers. In the presence of a linear stratification, the drag on the grid was found to be significantly larger than in the homogeneous case. This increase is interpreted as being due to the additional buoyancy force required to displace fluid elements in the wake of the grid from their equilibrium positions. A buoyancy drag has been defined as the additional drag force due to the stratification. The buoyancy drag coefficient is relatively insensitive to grid Reynolds number $Re_g = W_g M / \nu$ and is shown to be a function of overall Richardson number $Ri_o = N^2 M^2 / W_g^2$, where N is the buoyancy frequency of the stratification, W_g is the vertical velocity of the grid, M is the grid mesh size, and ν is the kinematic viscosity of the fluid. The additional drag force varies as $Ri_o^{1/2}$ suggesting that, as Ri_o increases, a larger proportion of energy imparted to the fluid by the grid is initially in the form of potential energy caused by the displacement of the isopycnal surfaces. A simple model of this process is described.

1 Introduction

Although the drag on a grid of bars submerged in a homogeneous fluid has been measured for many experimental configurations (see Sect. 2.2), the drag on a grid moving through a stratified medium has received less attention. The related problem of isolated bodies moving through a stratification has been studied in more detail due to a number of applications to naturally occurring flows. At low Reynolds numbers the drag on airborne particles in the atmosphere and particles in the upper ocean moving

parallel to a density gradient has an important effect on their vertical distribution (Srđić-Mitrović et al. 1999; Hanazaki and Torres 2000). Applications at larger Reynolds numbers include the rise of thermals (Warren 1960) and the buoyant rise of a nuclear cloud (McLaren et al. 1973) in a stably stratified atmosphere. A selection of studies of the drag on isolated objects moving vertically in a stratified fluid is discussed below.

The drag force acting on a sphere moving vertically through a stratified fluid has been considered in numerical simulations by Hanazaki and Torres (2000) and Torres et al. (2000). These simulations show that the drag on the sphere increases as the stratification of the fluid increases. The increase in drag is attributed to the generation of a ‘rear jet’ (in the opposite direction to the sphere), which forms when the isopycnal surfaces, deformed by the passage of the sphere, return to their original positions. An equivalent interpretation is that the drag is due to the work required to create the potential energy associated with the departure of the isopycnals from horizontal. In a related study of dense particles settling through a diffuse density interface, Srđić-Mitrović et al. (1999) found that under certain conditions the drag on a particle can be an order of magnitude larger when falling through the interface compared to the drag when moving through the homogeneous layers above and below.

The drag on an object moving parallel to a constant density gradient has been calculated for an inviscid flow by Eames and Hunt (1997). In this problem, a drag force is generated due to the action of the baroclinic torque and vortex stretching produced by the density gradient. The study does not, however, consider the effects of buoyancy on the drag force. (The baroclinic torque is a result of an object moving in a non-Boussinesq fluid rather than a gravitational effect.) Despite these investigations, the effects of stable stratification on the drag of a vertically moving body are not understood.

In the present study, a set of experiments was carried out in which a grid was suspended beneath a buoyant float. This arrangement was then submerged in a stratified fluid and allowed to rise freely under the action of buoyancy. After an initial acceleration period, following the release of the arrangement from rest, the drag on the grid and float is balanced by their combined buoyancy forces.

In Sect. 2 the drag force on a grid moving in a homogeneous fluid is measured. The increased buoyancy force on a grid submerged in a salt solution, above that in fresh water, is considered in Sect. 3. In Sect. 4 the drag force on the grid in a linearly stratified fluid is measured, and this is modelled in Sect. 5. Section 6 summarises this discussion.

Received: 14 August 2001 / Accepted: 27 December 2002
Published online: 7 May 2003
© Springer-Verlag 2003

R.C. Higginson (✉), S.B. Dalziel, P.F. Linden
Department of Applied Mathematics and Theoretical Physics,
University of Cambridge, Silver Street, Cambridge, CB3 9EW, UK
E-mail: rch26@damtp.cam.ac.uk

Present address: P.F.Linden
Department of Mechanical and Aerospace Engineering,
University of California, San Diego, 9500 Gilman Drive, La Jolla,
CA, 92093-0411, USA

2

Drag in a homogeneous fluid

In this section we describe measurements of the drag on a grid (and float) in a homogeneous fluid. If D_{float} and D_{grid} are the drag forces on the float and grid, respectively, and F_{arr} is the buoyancy force in fresh water acting on the grid and float (i.e., the weight of the grid and float subtracted from their combined upthrust in fresh water), then for the grid moving at constant velocity in fresh water

$$F_{\text{arr}} = D_{\text{float}} + D_{\text{grid}}, \quad (1)$$

where D_{float} and D_{grid} are each functions of Reynolds number.

Rewriting Eq. (1) in terms of the drag coefficient of the float C_{float} and the drag coefficient of the grid C_D in the standard way (see, for example, Hoerner 1965) gives

$$F_{\text{arr}} = \frac{1}{2} \rho_0 C_{\text{float}} W^2 A_{\text{float}} + \frac{1}{2} \rho_0 C_D W_g^2 A_{\text{grid}}, \quad (2)$$

where A_{float} and A_{grid} are the solid areas of the float and grid, respectively, ρ_0 is the density of fresh water, W_g is the velocity of the grid, and W is the velocity of the float. (With the grid attached to the float $W=W_g$.) This assumes that there is negligible interaction of the drag on the two objects.

By incrementally changing the buoyancy of the float with and without the grid attached, the drag coefficient of both objects was measured over a range of Reynolds numbers.

2.1

Apparatus for drag measurement

The grid used in these drag experiments consisted of four strips of 1 mm thick aluminium sheet, which were arranged as shown in Fig. 1a, having a mesh size $M=9.8$ cm. The length of each strip was approximately equal to twice the mesh size (2×9.8 cm), and each had a width of 2.0 cm. The float consisted of two 'ping-pong' balls (diameter 3.8 cm) placed in series. A threaded steel rod passed

through the centre of the balls and extended 4.5 cm behind the float. The rod was loaded with steel washers (5 mm or 9 mm diameter). The buoyancy of the float could be changed by the removal or addition of a washer, and this change was calculated by measuring both the weight and upthrust (in fresh water) of the washers using a set of electronic scales. Lengths of 0.3 mm diameter nylon thread were used to connect the float to each corner of the grid (Fig. 1b). The total height of the arrangement was 51.5 cm. It is assumed that the length of the thread connecting the float and grid was sufficient such that the interaction of flow around the two objects was negligible.

The experiments were performed in a deep tank; a total depth of 130 cm ensured that terminal velocity was achieved. The tank had a large base area (75 cm \times 75 cm) to avoid interaction between the grid and the tank walls.

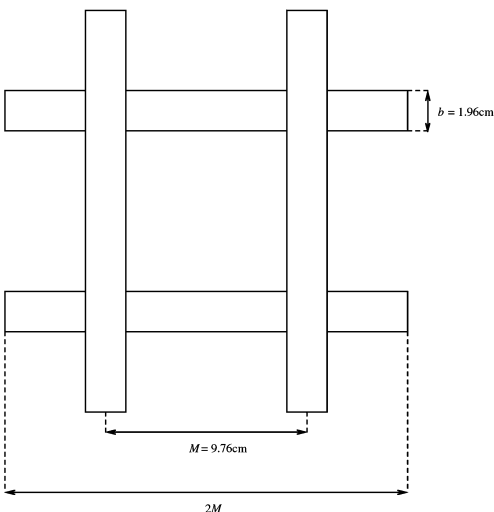
2.2

Evaluation of drag coefficients

The drag coefficient of the float was measured without the grid attached and is shown in Fig. 2. The drag coefficient of the grid (determined from Eq. (2) using the value of C_{float} as above) is plotted in Fig. 3.

In these plots different buoyancy forces F_{arr} were created by the removal of between one and eight steel washers (relative to neutral buoyancy). The velocity of the arrangement and the solid areas of the float and grid were used to evaluate C_{float} and C_D , respectively. To determine the velocity of the grid or float, time series of the vertical position of each object were made and the gradient calculated using a linear least-squares fit algorithm. A typical time series is shown in Fig. 4 and is described in more detail in Sect. 4. For the purposes of calculating the drag coefficients, the mean velocity from three traverses was used. The horizontal and vertical error bars shown in both plots are based on the maximum difference between the three velocities. In both figures the drag coefficient is plotted against the Reynolds number of the corresponding object. The velocity scale used in the Reynolds number was

a) Small Grid



b) Float and Grid Arrangement

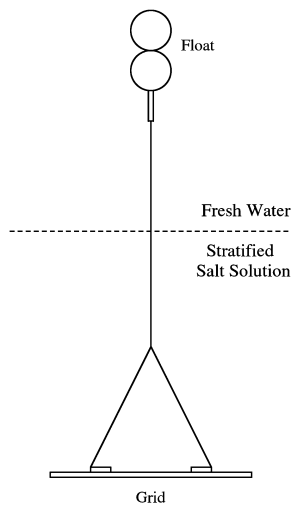


Fig. 1. a Plan view of the grid used in the drag experiments. b A schematic diagram of the float and grid arrangement used in the drag experiments, together with their positions relative to the stratified fluid surrounding them. The depth of each of the two fluid layers was approximately 65 cm

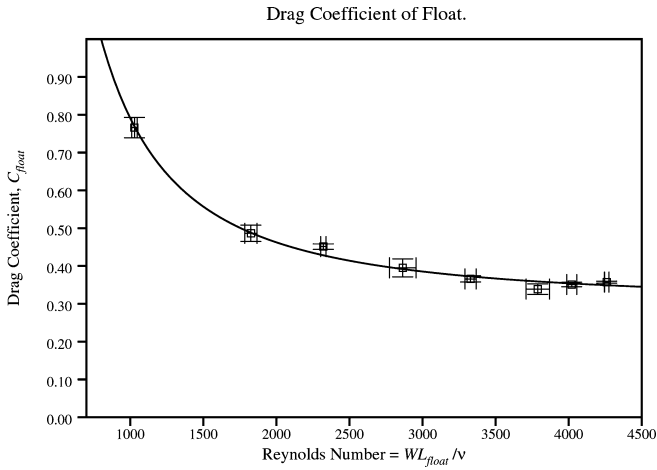


Fig. 2. The drag coefficient of a buoyant float $C_{\text{float}} = D_{\text{float}} / \frac{1}{2} \rho_0 W^2 A_{\text{float}}$ plotted as a function of the Reynolds number WL_{float}/v . The float was constructed from two hollow spheres in series and was allowed to rise freely through a tank containing fresh water. In calculating the mean velocity of the float, velocity data from three float traverses was used and the maximum difference between these is reflected in both the horizontal and vertical error bars

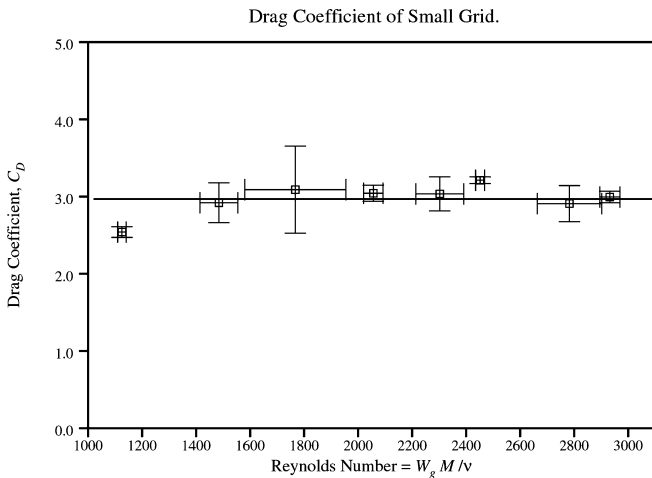


Fig. 3. The drag coefficient of a mesh of bars $C_D = D_{\text{grid}} / \frac{1}{2} \rho_0 W_g^2 A_{\text{grid}}$ plotted as a function of the Reynolds number, $W_g M/v$. The grid (Fig. 1a) was lifted through a tank containing fresh water using a small buoyant float (Figs. 1b and 2). Error bars are calculated in the same way as those in Fig. 2

the velocity of the grid W_g or the float W , and the relevant length scale used was the mesh size of the grid M , or in the case of the float, its diameter $L_{\text{float}} (=3.8 \text{ cm})$.

It is seen from Fig. 2 that the drag coefficient of the float C_{float} is a decreasing function of Reynolds number. This is a similar trend to the drag coefficient of a sphere over the same Reynolds number range (examples may be found in Batchelor (1967) and Massey (1983)). However, C_{float} is slightly larger than previous measurements of the drag coefficient of a sphere, which is attributed to the more complex shape of the float. The curve $3.09 \times 10^4 Re^{-1.6} + 0.3$ in Fig. 2 provides a reasonable fit to the data. Absolute values of the drag force on the float and grid (not shown)

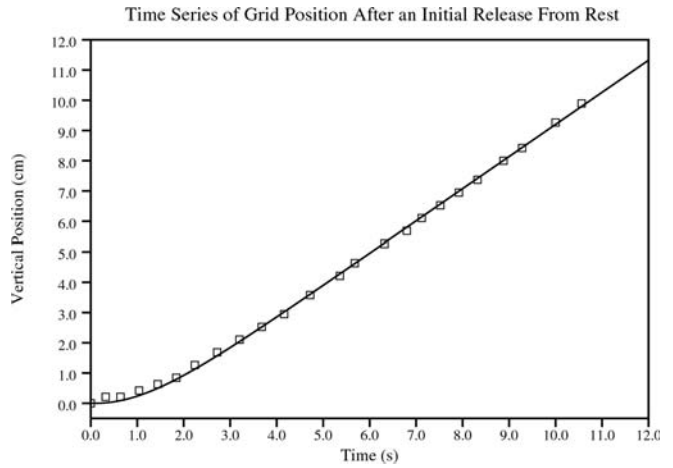


Fig. 4. The grid arrangement was released from rest and allowed to rise freely under the action of buoyancy. The vertical position h of the grid is plotted as a function of time t . The axes have been set so that the grid release coincides with $(h,t)=(0,0)$. It is seen that the grid accelerates from rest to a constant velocity approximately equal to 1.06 cm s^{-1} . The continuous line shows the solution to Eq. (10) with W_g replaced by dh/dt

indicate that the drag on the grid was between 30 and 60 times larger (depending on grid speed) than that on the float, and thus the precise behaviour of C_{float} was not crucial.

The drag coefficient of the grid C_D (Fig. 3) was approximately constant and was equal to 2.97 ± 0.18 over the range of Reynolds numbers $1000 \lesssim Re_g \lesssim 3000$. The finding that C_D is approximately independent of Re_g is consistent with arguments by Fox and McDonald (1973) and Massey (1983) that for objects with sharp edges (such as the aluminium strips used to make the grid in the present experiments) boundary layer separation always occurs at the edges for Reynolds numbers greater than about 100 (Massey 1983). As a result, the drag is proportional to the square of the velocity, and C_D is independent of Re_g . A similar independence of Re_g (over a similar range as investigated here) was found by Rottman and Britter (1986), who measured a drag coefficient for a horizontally traversed grid with a mean value of 1.4. However, Rottman and Britter used the total area of fluid circumscribed by the grid to nondimensionalise their drag data, whereas we use only the solid area. A quantitative comparison is obtained by dividing their drag coefficient by the solidity of the grid σ . The result is a rescaled drag coefficient of 3.5, which is larger than, but within 20% of the present value. Similarly, dividing the drag coefficient by the solidity of a freely falling grid (in fresh water) in the experiments of Linden (1980) gives a drag coefficient of 4.44 (for $Re_g = 5 \times 10^3$). In wind-tunnel experiments by Comte-Bellot and Corrsin (1966), the drag coefficient was $C_D = 4.53$ (Naudascher and Farrell 1970). However, these experiments were performed at Reynolds numbers ($Re_g \approx 34,000$) significantly larger than those considered in the present experiments. The smaller drag coefficient measured in the present work compared to those found by the aforementioned authors is thought to be due mainly to the overall size of the present grid (a total span of two mesh lengths) and the large clearance between the grid and the walls of

the tank, although it may also be affected by the grid solidity. Measurements by Bearman (1978) suggest that the drag on a bar of rectangular cross-section is relatively insensitive to its thickness. It is therefore likely that the thickness of the grid used in the present experiments (1 mm, see Sect. 3) was not responsible for its smaller drag coefficient.

For grids of circular rods, the drag coefficient C_D was found to be in the range $2.12 \leq C_D \leq 2.18$ in a collection of grid turbulence experiments collated by Naudascher and Farrell (1970). For these experiments $650 \leq Re_g \leq 11,000$ and $0.338 \leq \sigma \leq 0.376$. For the present experiment $1000 \lesssim Re_g \lesssim 3,000$ (Fig. 3), and $\sigma \approx 0.36$. The values of C_D in this range are smaller than the present value; however, this may be expected since flow separation is likely to be more severe for the sharp edges of a rectangular bar resulting in a higher drag (Comte-Bellot and Corrsin 1966). Based on the experiments reviewed above, the drag coefficient, $C_D=2.97$, for the present experiments appears to be consistent with the type of grid used.

3 Analysis of the buoyancy force

In a stably stratified fluid, the buoyancy of the grid is expected to decrease as the grid rises from surroundings of one density into surroundings of a lower density. Thus, to properly investigate the drag on the grid in a stratified fluid it is necessary to consider this effect in more detail. For the low grid speeds used in the present drag experiments, differences in salinity (and hence density) produced an upthrust on the grid that was significant compared to the small drag forces. To quantify this effect, experiments were performed in a tank filled with a step stratification made up of two homogeneous layers. The step stratifications had fresh water at the top (surrounding the float at all times) and dense salt solution (with $\rho=1.03 \text{ g/cm}^3$ or $\rho=1.06 \text{ g/cm}^3$) at the bottom (surrounding the grid at all times), with each layer having a depth of approximately 65 cm. Rewriting Eq. (1) to include the additional buoyancy force B_{grid} acting on the grid because of a density difference across the step of $\Delta\rho$ gives

$$F_{\text{arr}} + B_{\text{grid}} = D_{\text{float}} + D_{\text{grid}}. \quad (3)$$

Since F_{arr} is a known function of the number of steel washers attached to the float, and D_{float} and D_{grid} are measured empirical functions of Reynolds number, B_{grid} may be determined from the velocities measured in the step stratification experiments. For both objects, the absolute drag was found to be modelled closely using curves of the form $k_1 Re^2 + k_2 Re$, where k_1 and k_2 are dimensional constants. Calculating the grid velocity (as described in Sect. 2.2) for the two known density steps, the additional buoyancy was found to be $B_{\text{grid}} (\text{Newtons}) = (0.144 \pm 0.021) \Delta\rho (\text{g/cm}^3)$.

It is noted that B_{grid} may be written in terms of the volume of the grid V_{grid} , thus

$$B_{\text{grid}} = g \Delta\rho V_{\text{grid}}, \quad (4)$$

where g is the acceleration due to gravity.

Estimating the volume of the grid using Eq. (4) and B_{grid} measured in the step stratification experiments leads to $V_{\text{grid}} = 14.7 \text{ cm}^3$. This estimate compares well with the volume of the grid measured directly, equal to 15.3 cm^3 (there being only 4% difference between the two values), providing support for the accuracy of the drag measurements.

To minimise the direct effects of density variation on the grid motion, it is noted from Eqs. (2) and (4) that, for a given value of F_{arr} , the ratio of the buoyancy force B_{grid} to the drag on the grid D_{grid} is

$$\frac{B_{\text{grid}}}{D_{\text{grid}}} = \frac{g \Delta\rho A_{\text{grid}} T_{\text{grid}}}{\frac{1}{2} \rho_0 C_D W_g^2 A_{\text{grid}}}, \quad (5)$$

where T_{grid} is the thickness of the grid, and $A_{\text{grid}} T_{\text{grid}} = V_{\text{grid}}$ is the grid volume. Bearman (1978) reports that C_D is only a weakly increasing function of T_{grid} , and therefore the enhanced buoyancy B_{grid} may be reduced by decreasing the thickness of the grid. The grid used in the drag experiments reported here had a relatively small thickness of 1 mm compared to the bar width of 20 mm.

4 Measurement of the buoyancy drag

To measure the effects of a constant density gradient on the drag of the grid, stratifications were prepared in which a layer of fresh water (containing the float) overlay a linearly stratified layer (containing the grid), with each layer having a depth of approximately 65 cm (Fig. 1b). The linear stratifications used in these experiments were created using a 'double-bucket' technique (Oster 1965), and the buoyancy frequencies $N = [g/\rho_0 (\partial\rho/\partial z)]^{1/2}$ were determined from a set of six density samples taken from known depths. If D_{strat} is the additional drag due to the vertical transport of buoyant fluid by the grid, then rewriting Eq. (3) to include this term gives

$$F_{\text{arr}} + B_{\text{grid}} = D_{\text{float}} + D_{\text{grid}} + D_{\text{strat}}. \quad (6)$$

It is noted that no additional buoyancy term is required for the float in this equation as it continuously remains immersed in fresh water.

4.1 Force analysis for an accelerating grid

Implicit in Eq. (6) is the assumption that acceleration terms are negligible and the forces acting on the system (grid and float) are in balance. However, for the grid traversing a linear stratification, B_{grid} (and hence D_{float} , D_{grid} and D_{strat}) are expected to vary in time. Thus the velocity of the grid is not constant and acceleration terms may be significant.

As D_{strat} is unknown, it is not possible to evaluate the combined effect of the acceleration terms directly by summing the forces acting on the grid arrangement. To justify the force balance used in Eq. (6), time scales for the change in buoyancy force acting on the grid and the velocity adjustment of the grid to its surroundings are compared. If the forces acting on the arrangement adjust (become balanced) at a rate significantly faster than the rate of change caused by the grid moving

into surroundings of different density, then the acceleration terms will be small compared to the individual forces.

For the grid traversing a stratified fluid with constant N , the balance of forces acting on it will be altered through changes in the additional buoyancy force acting on the grid B_{grid} . If the forces are to balance, the combined drag on the grid and float must adjust so that no net force acts on the arrangement. The rate at which the forces acting on the arrangement become unbalanced is taken to be the rate at which B_{grid} changes due to the grid traversing a linear stratification. Since g and V_{grid} are constant, B_{grid} (defined by Eq. (4)) can only change because of the local density of the surrounding fluid. A quantity (with the units of inverse time) representing a rate for the change of local fluid density is

$$\left| \frac{d\rho}{dt} \right| / \rho_0 = \left| \frac{d\rho}{dz} \right| \frac{W_g}{\rho_0} = \frac{N^2}{g} W_g. \quad (7)$$

In order to estimate the rate at which the velocity of the grid (or the forces acting on the grid) adjusts to new surroundings, the acceleration of the grid in a homogeneous fluid is considered

$$F_{\text{arr}} - D_{\text{float}} - D_{\text{grid}} = m \frac{dW_g}{dt}, \quad (8)$$

where dW_g/dt is the acceleration of the grid arrangement, and m is its inertial mass, including the added mass of any fluid transported with the grid. It is assumed, for convenience, that the rate of the velocity adjustment in a stratified fluid is equal to the rate of velocity adjustment in a homogeneous fluid. In Sect. 3 it was noted that the absolute drag of the float or grid could be modelled using curves of the form $k_1 Re^2 + k_2 Re$, where k_1 and k_2 are constants. Using this result, the combined drag force acting on the grid arrangement (submerged in a homogeneous fluid) is approximated by

$$D_{\text{grid}} + D_{\text{float}} = \alpha W_g^2 + \beta W_g. \quad (9)$$

where α and β are constants.

Substituting Eq. (9) into Eq. (8) gives a first-order ordinary differential equation describing the acceleration of the grid. Solving this differential equation gives

$$e^{-2\alpha x t/m} = \left| \frac{W_g - W_\infty}{A \left(W_g + W_\infty + \frac{\beta}{\alpha} \right)} \right|, \quad (10)$$

where $W_\infty = (\sqrt{\beta^2 + 4\alpha F_{\text{arr}}} - \beta)/2\alpha$ is the grid velocity as $t \rightarrow \infty$ (obtained by solving Eq. (8) with the right side set to zero), $a = W_\infty + \beta/2\alpha$, and A is a constant of integration. Thus, the grid released from rest, say, would be expected to accelerate to W_∞ at a rate $O(2\alpha a/m)$. This rate will be taken as the rate of adjustment of the velocity of the grid as it moves into surroundings of different density. It is assumed that buoyancy does not significantly affect the rate of velocity adjustment of the grid as it moves from one region with local asymptotic velocity $W_{\infty(1)}$, the velocity as $t \rightarrow \infty$, to a new region with asymptotic velocity $W_{\infty(2)}$.

To evaluate the adjustment rate it is necessary to estimate m as defined by Eq. (8) relevant for a bluff body towed through a fluid of density ρ_0 . This mass is the summation of the inertial mass (of the combined float and grid) and the added mass m_a from fluid transported forward by the passage of the float and grid (Massey 1983, p 343; Lamb 1932). For an inviscid fluid, the added mass of an accelerating body represents the effective mass of the fluid that surrounds the body that must be accelerated with it, and depends on the body shape and orientation (Newman 1977). For a thin strip of width $2a$, moving through a fluid of density ρ_0 , perpendicular to its width, $m_a = \rho_0 \pi a^2 L$, where L is the length of the strip (Newman 1977; McCormick 1973). If the four bars making up the grid are each approximated by such strips, then the added mass of the grid is $m_a(\text{grid}) \approx 4\rho_0 \pi (b/2)^2 2M = 2\rho_0 \pi b^2 M$, where b is the width of each bar and $2M$ is the bar length. Thus to determine the adjustment rate, the effective mass m in Eq. (10) must be replaced by $m_{\text{arr}} + m_a(\text{grid})$, where m_{arr} is the inertial mass of the combined grid and float arrangement. The added mass of the float has been neglected in the estimate of m because its added mass is less than a tenth that of the grid.

As stated earlier, different values of F_{arr} were achieved by removing steel washers from the arrangement, which resulted in a range of adjustment rates $1.3 \text{ s}^{-1} \lesssim 2\alpha a/m \lesssim 3.8 \text{ s}^{-1}$, with the larger rates corresponding to the larger number of removed washers. The removal of the washers also resulted in a change in the inertial mass of the arrangement, $72.4 \text{ g} \leq m_{\text{arr}} \leq 74.3 \text{ g}$.

The accuracy of the estimates of the adjustment rate may be tested by comparing predictions of the initial acceleration of the grid with experimental measurements such as those presented in Fig. 4. This figure shows the vertical elevation of the grid h plotted against the corresponding time t for the grid released from rest (at $t=0$). The case shown here represents the slowest adjustment rate, where only one washer was removed, leading to a terminal velocity $W_\infty \approx 1.06 \text{ cm s}^{-1}$. Noting that the elevation of the grid h obeys $dh/dt = W_g$ and substituting this into Eq. (10) with the initial conditions $W_g=0$ and $h=0$ at $t=0$, we may solve the resulting ordinary differential equation to obtain $h(t)$. The solid line in Fig. 4 shows the curve given by $h(t)$ with a value for the adjustment rate of 1.1 s^{-1} . Evaluating the predicted adjustment rate, $2\alpha a/m = 1.3 \text{ s}^{-1}$, which is greater than but close to that in Fig. 4, validating the inclusion of the added mass contribution to m .

The rate of adjustment must be much faster than the rate at which the forces become unbalanced (see Eq. (7)) for the forces acting on the grid to be in approximate balance, hence

$$\Gamma = \frac{2\alpha a \rho_0}{m W_g} \left| \frac{d\rho}{dz} \right|^{-1} \gg 1. \quad (11)$$

Substituting for the maximum density gradient and velocities measured experimentally, we find $350 \lesssim \Gamma \lesssim 750$. It is assumed hereafter that these values of Γ are sufficiently large to satisfy Eq. (11) and consider the forces

to be in equilibrium, thus allowing the use of the force balance given by Eq. (6).

In contrast to the case of a linear stratification, acceleration terms were observed to be significant while performing the experiments in a step stratification (see Sect. 3), where $|d\rho/dz|$ can be large. In these experiments the grid was often observed to stop or temporarily reverse direction upon reaching the sharp salinity interfaces, as dense fluid carried into the upper layer settled under the action of gravity. It is therefore expected that Eq. (11) will not be satisfied in such cases. The salinity interfaces in the experiments were observed to be diffuse and had a width ~ 0.5 cm. Assuming that the density at the interface varied smoothly over this height, and that the motion at the interface can be approximated by the motion in a continuous stratification with a density gradient equal to the gradient of the diffuse interface, we find $6.6 \lesssim \Gamma \lesssim 8.0$, and it is not clear that Eq. (11) is satisfied. This suggests that the grid motion at a sharp density interface cannot be analysed using the simple force balance used here to study the motion in a linear stratification. Further discussion on the behaviour in a step stratification is beyond the scope of this paper.

4.2

Evaluation of the buoyancy drag

Before proceeding it is noted that time series of the grid position in a linear density gradient will differ from those in a homogeneous fluid because B_{grid} decreases as the grid rises into less dense fluid. For the linear stratifications studied here the measured time series were not linear, with h qualitatively appearing to have a $t^{1/2}$ dependence. It was found that each time series could be closely modelled with a curve of the form $h=c_1 t^{1/2}+c_2 t+c_3$ (where c_1 , c_2 , and c_3 are constants), which was differentiated to obtain the instantaneous grid velocity.

Using the known empirical functions for F_{arr} , D_{grid} , D_{float} , and B_{grid} , the buoyancy drag D_{strat} was calculated for two stratifications ($N=1.1 \text{ s}^{-1}$, 1.69 s^{-1}) and a range of grid

velocities. The results are shown in Fig. 5. Here the buoyancy drag D_{strat} (for two strengths of stratification) and the unstratified drag on the grid D_{grid} are plotted against the grid Reynolds number. The values of D_{strat} for different buoyancy frequencies N are distinct with D_{strat} increasing with N , thus showing that D_{strat} is dependent on the overall Richardson number Ri_o . For the relatively low grid speeds here, D_{strat} is greater than D_{grid} for both values of N , suggesting that much of the work done by the grid is converted initially to potential energy rather than kinetic energy. It can also be seen from Fig. 5 that D_{strat} is approximately proportional to Re_g for each value of N , and the data are plotted together with linear least squares fits for the two stratifications.

The D_{strat} data for both stratifications appears to be grouped into sets of individual curves superimposed on one another, and it is noted that each of these sets corresponds to the range of W_g observed from a single grid release. Some patterns can be seen in the scatter of the data, particularly between the data from different grid releases. This may be a Reynolds number effect since the grid velocity decreases with height, although it could be a systematic feature of the error in the individual forces used in Eq. (6) to estimate D_{strat} . Another possible source of systematic error is in the estimate of D_{grid} . It is recalled that D_{grid} was measured in experiments performed in fresh water and modelled using Eq. (9); however, for the dense salt solutions used in the stratified experiments it is not clear that the flow may be considered to be Boussinesq. In the regions of each stratification where the local density is significantly greater than that of fresh water (up to 15% for the $N=1.69 \text{ s}^{-1}$ case) the unstratified component of the total drag is likely to be greater than the fresh water measurement (for the same value of Re_g), thus Eq. (9) provides an underestimate of D_{grid} . Using Eq. (6) it was calculated that an underestimate of D_{grid} of 15% could account for an overestimate of D_{strat} of up to 6% in regions of high density and may explain some of the pattern seen in the data. However, reducing the values of D_{strat} by 6%

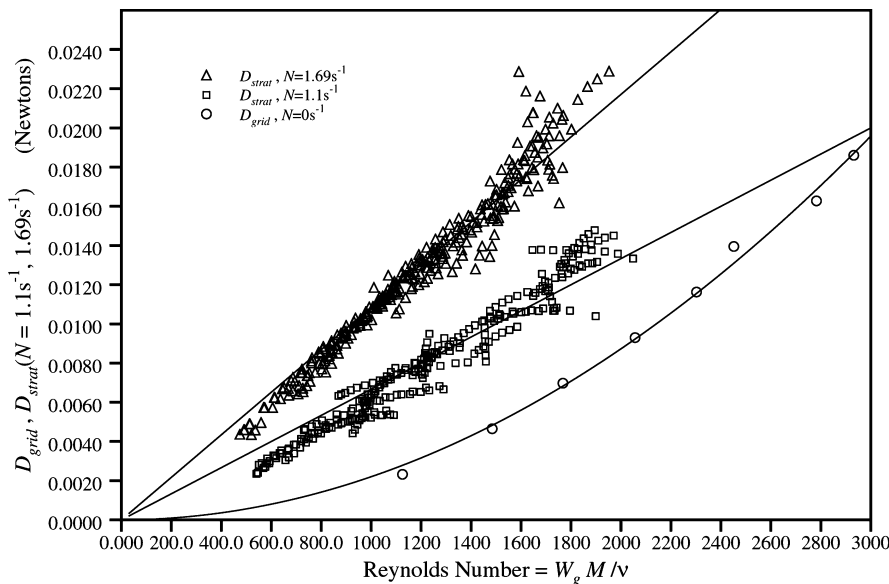


Fig. 5. The additional drag force (defined by Eq. (6)) acting on a grid moving vertically through a linear stratification is shown here for two values of the buoyancy frequency N . Also shown is the drag on the grid moving through fresh water. All are plotted against Reynolds number $Re_g=W_g M/\nu$. The unstratified drag has been fitted with a curve of the form $\alpha Re_g^2+\beta Re_g$, while the D_{strat} data is found to be approximately proportional to Re_g . Since the range in the experimental data is clear from the plot, error bars have been omitted for the D_{strat} data

for data corresponding to regions of high local density was found to increase the scatter in the data, suggesting that non-Boussinesq effects are not the major component of the observed scatter.

In addition to the standard parameters used to nondimensionalise the unstratified drag (D_{grid}), D_{strat} may also depend on other parameters associated with the stratification, e.g., $d\rho/dz$ and g . Thus, there is no unique nondimensionalisation including some or all of the available quantities. However, to simplify the interpretation and discussion we follow the same framework as is used for homogeneous fluids and write the combined drag force D_{Total} as

$$D_{\text{Total}} = D_{\text{grid}} + D_{\text{strat}} = \frac{1}{2}\rho_0(C_D + C_S)W_g^2A_{\text{grid}}, \quad (12)$$

noting that the stratification (buoyancy) drag coefficient C_S may be a function of Re_g and Ri_o . This approach is similar to that used by Srdić-Mitrović et al. (1999) to nondimensionalise their stratification drag in studying the motion of negatively buoyant particles moving through homogeneous and stratified layers. This nondimensionalisation is also adopted in the present study, as it allows for direct comparison of the magnitudes of both the stratified and unstratified drag coefficients.

For sufficiently high Re_g and Schmidt numbers, we may anticipate that C_S will only be a function of overall Richardson number, $Ri_o = N^2M^2/W_g^2$. This is demonstrated in Fig. 6, which plots the dimensionless buoyancy drag coefficient C_S as a function of Ri_o , and suggests a power law relationship of the form

$$C_S = \frac{D_{\text{strat}}}{\frac{1}{2}\rho_0W_g^2A_{\text{grid}}} = kRi_o^p, \quad (13)$$

for constants k and p . A linear least-squares fit suggests $p=0.47$ and $k=1.034$. This fit is plotted as a solid line with the data in Fig. 6. We see that plotting the data in this way provides an adequate collapse, supporting the assumption that there is no additional dependence on Reynolds

number. Error bars have been omitted from this plot since the range in the experimental data is clear.

As with Fig. 5 some pattern can be seen in the spread of the data in Fig. 6. The possibility of non-Boussinesq effects was investigated for this data, namely through the choice of appropriate reference density ρ_0 in Eqs. (12) and (13). Although the density used was that of fresh water (consistent with the measurements of C_D), larger densities may be more applicable for data corresponding to regions of the stratifications of greater density. However, as with Fig. 5, adjusting these data did not improve the collapse.

5 Modelling the behaviour of C_S

We now present a simple scaling argument consistent with the power law relationship between C_S and Ri_o given by Eq. (13). The scaling is not intended to explain the complex dynamics of the flow that results from the passage of the grid, but simply to illuminate the mechanism responsible for the drag.

Consider the grid travelling upwards through a linearly stratified fluid with constant velocity W_g . As the grid moves, isopycnal surfaces, which are initially horizontal, are displaced upward in the wake of the grid. In the absence of any mixing, the restoring force F per unit volume of a fluid element displaced vertically a distance l in a linearly stratified fluid with mean density gradient $d\bar{\rho}/dz$ is

$$F = gl \frac{d\bar{\rho}}{dz}. \quad (14)$$

We propose that this restoring force is the main contribution to D_{strat} . Additional experiments (Higginson 2000) were performed to estimate the internal wave energy in the wake of the grid in a linear stratification, and based on these measurements and comments by Hanazaki and Torres (2000), it is believed that the contribution to the drag on the grid due to internal waves (Warren 1960) is relatively minor.

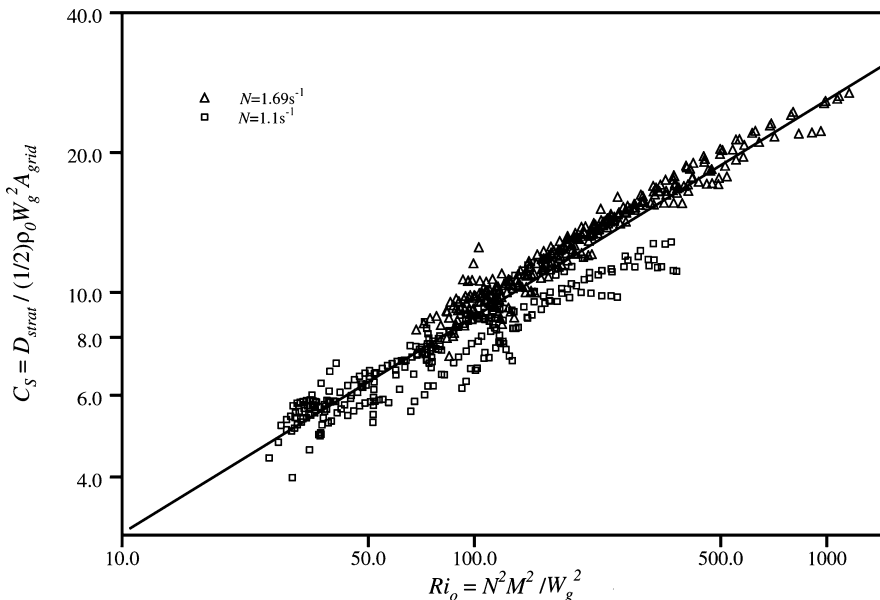


Fig. 6. The buoyancy drag coefficient $C_S = D_{\text{Total}}/\frac{1}{2}\rho_0W_g^2A_{\text{grid}}$ is found for the present data to collapse onto a single curve when plotted against the overall Richardson number $Ri_o = N^2M^2/W_g^2$. A curve of the form $C_S = kRi_o^{0.47}$ is also plotted, with the constant $k=1.034$. Since the range in the experimental data is clear from the plot, error bars have been omitted

In order to calculate the total restoring force resulting from the fluid displaced by the grid, estimates of the volume of fluid displaced and the height to which it is lifted are required. Associated with the added mass m_a of a body is its 'drift volume' V_{drift} . The drift volume of a body (Darwin 1953; Yih 1985) is the (finite) volume of fluid transported in the direction of propagation as a result of its motion and is equal to the volume m_a/ρ_0 , where ρ_0 is the density of the surrounding fluid (Eames and Flör 1998). For the vertically traversing grid considered here it is assumed that the volume corresponding to the displaced isopycnal surfaces is equal to the drift volume of the grid, $2\pi b^2 M$ (Sect. 4.1), and that this volume is relatively unaffected by the presence of a stratification. In particular, we assume that the primary effect of the stratification is to reduce the vertical extent of the isopycnal deformations, before buoyancy returns the displaced fluid elements to their equilibrium positions.

From dimensional arguments we expect that the maximum displacement of the isopycnal surfaces will scale as $l \approx \gamma W_g/N$, where γ is a constant $O(1)$. This scaling may be obtained by equating the initial vertical kinetic energy per unit volume of the fluid elements perturbed by the grid $\frac{1}{2}\rho_0 w^2$ (assumed to be proportional to $\frac{1}{2}\rho_0 W_g^2$) to the resultant potential energy change per unit volume caused by the fluid displacements $g/2(\partial\bar{\rho}/\partial z)l^2$ (Pearson et al. 1983).

From Eq. (14) an estimate of the total gravitational restoring force D_{strat} acting on the grid may now be written

$$D_{\text{strat}} \approx g \frac{\gamma W_g}{N} \frac{\partial\bar{\rho}}{\partial z} 2\pi b^2 M = 2\pi\gamma\rho_0 b^2 N M W_g. \quad (15)$$

Using this estimate, the buoyancy drag coefficient C_S may be expressed as

$$C_S = \frac{D_{\text{strat}}}{\frac{1}{2}\rho_0 W_g^2 A_{\text{grid}}} \approx \frac{4\pi\gamma b^2 N M}{A_{\text{grid}} W_g} = \frac{4\pi\gamma b^2}{A_{\text{grid}}} Ri_o^{1/2} \approx \gamma(0.35) Ri_o^{1/2}. \quad (16)$$

Comparison of Eq. (16) and the empirical relationship Eq. (13) shows that the exponents of Ri_o are in close agreement. This suggests that the above scaling argument justifies the use of a power law fit to the C_S data. Also, since γ is an $O(1)$ constant, the value of $k=1.034$ in Eq. (13) is consistent with this scaling. It is noted that since the present modelling is based only on the drift volume of the grid and a scaling for the maximum displacement of isopycnal surfaces, the $Ri_o^{1/2}$ dependence of C_S found for the present grid of bars is likely to apply to general symmetric objects traversing a constant density gradient.

6 Summary

Experiments were performed to calculate the drag forces on a grid moving vertically through a homogeneous and a stratified fluid. No such results for a stratified fluid have previously appeared in the literature. The drag coefficient C_D (defined by Eq. (2)) of the grid in a homogeneous fluid was found to be approximately equal to 2.97 over the range

of grid Reynolds numbers considered ($1,000 \lesssim Re_g \lesssim 3,000$). This value compares well with existing data (see Sect. 2.2). In a linearly stratified fluid, an additional drag coefficient C_S caused by the stratification (defined by Eq. (12)) was introduced and was found to be independent of Re_g but was an increasing function of the overall Richardson number, approximately as $Ri_o^{1/2}$ (given by Eq. (13)). This Richardson number dependence is found to be consistent with a simple model discussed in Sect. 5. Using an estimate of the fluctuating potential energy and kinetic energy caused by internal waves from particle tracking and salinity probe measurements it was found (Higginson 2000) that approximately 5% of the energy supplied to the fluid by the grid went directly into exciting internal waves, for an overall Richardson number of 134.6. This suggests that wave drag (Warren 1960), although undoubtedly a function of Ri_o , is a relatively small component of the buoyancy drag.

References

- Batchelor GK (1967) An introduction to fluid dynamics. Cambridge University Press, Cambridge
- Bearman PW (1978) Some effects of free-stream turbulence and the presence of the ground on the flow around bluff bodies. In: Sovran G, Morel T, Mason WT Jr (eds) Aerodynamic drag mechanisms of bluff bodies and road vehicles. Plenum, New York
- Comte-Bellot G, Corrsin S (1966) The use of a contraction to improve the isotropy of grid-generated turbulence. *J Fluid Mech* 25:657–682
- Darwin C (1953) Note on hydrodynamics. *Proc Camb Phil Soc* 49:342–354
- Eames I, Hunt JCR (1997) Inviscid flow around bodies moving in weak density gradients without buoyancy effects. *J Fluid Mech* 353:331–355
- Eames I, Flör J-B (1998) Fluid transport by dipolar vortices. *Dyn Atmos Oceans* 28:93–105
- Fox RW, McDonald AT (1973) Introduction to fluid mechanics. Wiley, New York
- Hanazaki H, Torres CR (2000) Jet and internal waves generated by a descending sphere in a stratified fluid. In: Lawrence GA, Pieters R, Yonemitsu N (eds) Proceedings of the 5th international symposium on stratified flows
- Higginson RC (2000) Turbulence and mixing in a stratified fluid. PhD thesis, University of Cambridge, UK
- Hoerner SF (1965) Fluid-dynamic drag. Hoerner Fluid Dynamics, Brick Town, NJ
- Lamb H (1932) Hydrodynamics, 6th edn. Cambridge University Press, Cambridge
- Linden PF (1980) Mixing across a density interface produced by grid turbulence. *J Fluid Mech* 100:691–703
- Massey BS (1983) Mechanics of fluids, 5th edn. Van Nostrand Reinhold, Wokingham UK
- McCormick ME (1973) Ocean engineering wave mechanics. John Wiley and Sons, Inc
- McLaren TI, Pierce AD, Fohl T, Murphy BL (1973) An investigation of internal gravity waves generated by a buoyantly rising fluid in a stratified medium. *J Fluid Mech* 57:229–240
- Naudascher E, Farell C (1970) Unified analysis of grid turbulence. *Proc ASCE, J Eng Mech Div* 96:121–141
- Newman JN (1977) Marine hydrodynamics. MIT Press, Cambridge, MA
- Oster G (1965) Density gradients. *Sci Am* 213:70–76
- Pearson HJ, Puttock JS, Hunt JCR (1983) A statistical model of fluid-element motions and vertical diffusion in a homogeneous stratified turbulent flow. *J Fluid Mech* 129:219–249
- Rottman JW, Britter RE (1986) The mixing efficiency and decay of grid-generated turbulence in stably-stratified fluids. In: Proceedings of the 9th Australasian fluid mechanics conference, Auckland, New Zealand, 8–12 Dec 1986

- Srdić-Mitrović AN, Mohamed NA, Fernando HJS (1999) Gravitational settling of particles through density interfaces. *J Fluid Mech* 381:175–198
- Torres CR, Ochoa J, Castillo J (2000) Numerical experiments of stratified flow past an impulsively started sphere. In: Lawrence GA, Pieters R, Yonemitsu N (eds) Proceedings of the 5th international symposium on stratified flows, Vancouver, 10–13 July 2000
- Warren FWG (1960) Wave resistance to vertical motion in a stratified fluid. *J Fluid Mech* 7:209–229
- Yih CS (1985) New derivations of Darwin's theorem. *J Fluid Mech* 152:163–172